Inorganic Chemistry

pubs.acs.org/IC

Article

Tuning Cobalt(II) Phosphine Complexes to be Axially Ambivalent

Jack Thomas-Colwell, Arvin Sookezian, Daniel A. Kurtz, Jeremy Kallick, Lawrence M. Henling, Troy A. Stich, Michael G. Hill, and Bryan M. Hunter*

Cite This: *Inorg. Chem.* 2022, 61, 12625−12634

Read Online

ACCESS | Metrics & More | Article Recommendations | Supporting Information

ABSTRACT: We report the isolation and characterization of a series of three cobalt(II) bis(phosphine) complexes with varying numbers of coordinated solvent ligands in the axial position. X-ray quality crystals of $[Co(dppv)_2][BF_4]_2$ (**1**), $[Co(dppv)_2(NCCH_3)][BPh_4]_2$ (**2**), and $[Co(dppv)_2(NCCH_3)_2][BF_4]_2$ (**3**) (dppv = *cis*-1,2-bis(diphenylphosphino)ethylene) were grown under slightly different conditions, and their structures were compared. This analysis revealed multiple crystallization motifs for divalent cobalt(II) complexes with the same set of phosphine ligands. Notably, the 4-coordinate complex **1** is a rare example of a square-planar cobalt(II) complex, the first crystallographically characterized square-planar Co(II) complex containing only neutral, bidentate ligands. Characterization of the different axial geometries via EPR and UV−visible spectroscopies showed that there is a very shallow energy landscape for axial ligation. Ligand field angular overlap model calculations support this conclusion, and we provide a strategy for tuning other ligands to be axially labile on a phosphine scaffold. This methodology is proposed to be used for designing cobalt phosphine catalysts for a variety of oxidation and reduction reactions.

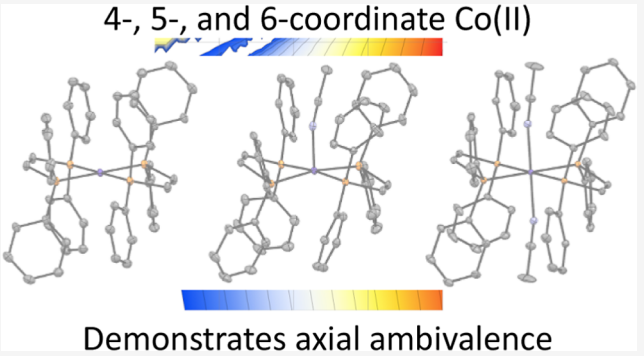

INTRODUCTION

Cobalt complexes have been studied extensively as relatively earth-abundant (~25,000 times more abundant than Rh or Ir)[1] redox catalysts for electrochemical applications.[2−5] In the case of multielectron activation of small molecules, tuning substrate and product binding to the catalytic center is critical: substrate binding that is too weak can result in large electrocatalytic overpotentials, while product binding that is too strong negatively affects the overall reaction kinetics.[6] Because of this, complexes which can reversibly bind ancillary ligands are of particular interest. The square-planar Vaska's complex, $IrCl(CO)[P(C_6H_5)_3]_2$, for example, is well-known to reversibly bind substrates such as dioxygen via oxidative addition.[7] However, the scarcity of third-row transition metals complicates the use of iridium for most large-scale applications.

Cobalt complexes featuring phosphine ligands (e.g., dppv, *cis*-1,2-bis(diphenylphosphino)ethylene) have also been reported to form 1:1 dioxygen adducts under a variety of conditions, albeit irreversibly.[8] These adducts are best described as side-bound cobalt(III)-peroxo species. For example, the brown, 6-coordinate complex $[Co(dppv)_2O_2][BF_4]$ can be prepared by dissolving $[Co(dppv)_2][BF_4]$ in CH_2Cl_2 in the presence of air, by adding dppv to an oxygenated solution of $[Co(H_2O)_6][BF_4]_2$ in acetone, or by bubbling air through a refluxing methanolic solution of $[Co(dppv)_2][BF_4]_2$. Interestingly, similar reactivity is not observed in complexes of the analogous bidentate ligand dppe (1,2-bis(diphenylphosphino)ethane).[8] It has been proposed that the more rigid dppv backbone allows for less steric hindrance of the axial position, though there is less structural information about cobalt dppv complexes in the literature. Although there are nearly 300 structures of M(dppv) complexes in the Cambridge Structural Database, only 59 are $M(dppv)_2$ structures and only 27 are of M = groups 9, 10, and 11.[9] None of the cobalt structures are 4-coordinate, even though the d^8 Ni(II) complex is square-planar.[10]

In our recent work on d^6−d^{10} cobalt complexes of dppv, we found that the d^7 $Co^{II}(dppv)_2^{2+}$ core crystallizes with one axial ligand (acetonitrile), generating a pseudo-square pyramidal geometry which we previously reported (**2**).[11] Herein, we further report that the core also crystallizes with 0 or 2 axial ligands (**1** and **3**), and we provide the structural characterization of each of these complexes. The former is a structure of 4-coordinate divalent $Co(dppv)_2^{2+}$ in a rigidly planar geometry. This is a rare (if not unprecedented) example of 4-coordinate Co(II) with bidentate redox-innocent ligands. The ability of $Co(dppv)_2^{2+}$ (**1**) to crystallize with or without

Received: May 6, 2022
Published: August 3, 2022

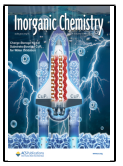

https://doi.org/10.1021/acs.inorgchem.2c01562
Inorg. Chem. 2022, 61, 12625−12634

axial ligands suggests that this cobalt cation is energetically precarious. This behavior is reminiscent of the work done in 1964 by Langford and Gray, in which anionic square-planar cobalt complexes with redox-active dithiolate ligands were interconvertible between 4-, 5-, and 6-coordinate environments upon addition of certain ligand(s).[12] We have analyzed the electronic structure of the multiple coordination environments using electron paramagnetic resonance (EPR) spectroscopy, UV−visible spectroscopy, and electrochemical measurements. To explore the underlying structural elements that give rise to the unusual axial-ligation ambivalence of this complex, we have developed a simple ligand-field model based on angular overlap calculations. This model maps out energy landscapes for 6- versus 5- versus 4-coordinate ML_4 cores as a function of readily tunable parameters, such as σ and π ligand donor strength and L−M−L "bite angles," providing a qualitative predictive tool for designing specific metal−ligand combinations engineered for the reversible binding of specific substrates.

EXPERIMENTAL SECTION

Materials and Methods. All reagents were purchased from Sigma-Aldrich unless otherwise stated.

All compounds were synthesized air-free using Schlenk techniques under argon. All solvents were dried using molecular sieves and thoroughly degassed prior to use.

Synthesis of 4-Coordinate $[Co(dppv)_2][BF_4]_2$ (1). **1** was prepared by dissolving cobalt(II) tetrafluoroborate hexahydrate (0.100 g, 0.294 mmol) in a minimal amount of dry, degassed acetone in a Schlenk flask. Two equivalents of the ligand, *cis*-1,2-bis-(diphenylphosphino)ethylene, were dissolved in a minimal amount of acetone in a separate Schlenk flask. The ligand solution was then cannulated into the cobalt solution, and the overall solution began turning yellow with a precipitate of the same color. The flask was cooled in a refrigerator for at least 1 h to maximize the amount of precipitation. The solid was filtered-off using a Schlenk frit and washed/dried several times with dry, degassed diethyl ether via cannulation, resulting in a 58% yield of a yellow solid. Complex **1** was crystallized by vapor diffusion of ether into a concentrated solution of $[Co(dppv)_2][BF_4]_2$ in acetone. The solid-state UV−vis reflectance spectrum of **1** has peaks at 900 and 1200 nm ($\varepsilon_{900} = 2\varepsilon_{1200}$, Supporting Information).

Synthesis of 5-Coordinate $[Co(dppv)_2(NCCH_3)_2][BPh_4]_2$ (2). **2** was prepared by dissolving compound **1** (0.100 g, 97.5 μmol) in a minimal amount of dry, degassed acetonitrile in a Schlenk flask (orange-colored solution). In a separate Schlenk flask, an excess (5−10 fold) of sodium tetraphenylborate was dissolved in a minimal amount of dry, degassed acetonitrile. With positive argon pressure, the cobalt solution was then cannulated into the sodium tetraphenylborate solution, and immediately a glittery orange precipitate was observed. The flask was stored in a refrigerator for at least an hour to maximize precipitation. Subsequently, the orange solid was filtered off using a Schlenk frit and washed/dried several times with dry, degassed diethyl ether via cannulation. A yield of 62% was obtained. The solid-state UV−vis reflectance spectrum of **2** has peaks at 700, 1200, and 1450 nm ($\varepsilon_{1200} = 2\varepsilon_{700} = 0.9\varepsilon_{1450}$, Supporting Information).

Synthesis of 6-Coordinate $[Co(dppv)_2(NCCH_3)_2][BF_4]_2$ (3). **3** was prepared by dissolving compound (**1**) (0.100 g, 97.5 μmol) in a minimal amount of dry, degassed acetonitrile in a Schlenk flask (orange-colored solution). The flask was capped and was stirred at room temperature for 5 min, during which the solution color changed from pale pink to dark orange. Over the next minute, 100 mL of ether was added to the orange solution while stirring vigorously, during which an orange precipitate formed. This solid was filtered in air and rinsed with minimal ether, dried under high vac, and was isolated in 65% yield. The solid-state UV−vis reflectance spectrum of **3** has peaks at 700, 1150, and 1400 nm ($\varepsilon_{1150} = 0.8\varepsilon_{1400} = 0.9\varepsilon_{700}$, Supporting Information).

Recrystallization of 5- and 6-Coordinate, $[Co^{II}(dppv)_2(MeCN)_y][BX_4]_2$, Where *X* is Ph or F and *y* is 1 or 2, Respectively. Compounds **2** and **3** were both recrystallized via vapor diffusion of diethyl ether into saturated solutions of **2** or **3** in acetonitrile.

UV/Visible/NIR Spectroscopy. Solution spectra were collected on a Cary 14 spectrometer in the dual-beam mode. Specular reflectance spectra were collected on a Cary 5000 spectrometer with an integrating sphere.

Single-Crystal X-ray Diffraction (1, 3). A suitable crystal was mounted on a polyimide MiTeGen loop with STP Oil Treatment and placed in the 100 K nitrogen stream of an Oxford Cryosystems 700 Series cryostream cooler. X-ray data for both compounds **1** and **3** were collected with a Bruker AXS D8 KAPPA APEX II diffractometer (Siemens KFF Mo 2 K-90 fine-focus sealed tube with Mo Ka = 0.71073 Å operated at 50 kV and 30 mA; TRIUMPH graphite monochromator; CCD area detector with a resolution of 8.33 pixels/mm) using a combination of ω- and φ-scans. All diffractometer manipulations, including data collection, integration, and scaling, were carried out using Bruker APEX3 software.[13] An absorption correction was applied using SADABS-2016/2.[14] The space group was determined, and the structure was solved by intrinsic phasing using XT-2014/5[15] (**1** and **3** are both in the monoclinic space group $P2_1/n$ (#14) with the cation on a center of symmetry). Refinement was full-matrix least-squares on F^2 using XL-2018/3.[16] All non-hydrogen atoms were refined using anisotropic displacement parameters. Hydrogen atoms were placed in idealized positions and the coordinates refined. The isotropic displacement parameters of all hydrogen atoms were fixed at either 1.2 or 1.5 (for methyl) times the U_{eq} value of the bonded atom.

EPR Spectroscopy. X-band EPR spectra were measured using a Bruker EMX spectrometer equipped with a cavity operating in the standard perpendicular mode, TE_{102}. Spectra at 77 K were collected using a finger Dewar filled with liquid nitrogen. Spectra at other temperatures were measured using an Oxford helium cryostat (ESR900). Due to the air-sensitive nature of these compounds in solution, the samples were prepared air-free under argon on a Schlenk line and immediately transferred into a custom air-free quartz Schlenk EPR tube. Simulations of the EPR spectra were performed using the EasySpin 5.2.28 toolbox[17] within the Matlab R2018a software suite (The Mathworks Inc., Natick, MA).

Certain ligand-field excited state energies can be estimated based on the shift of the observed *g*-value from the free electron *g*-value ($g_e = 2.0023$) using first-order perturbation theory formulas developed by Pryce.[18] Specifically, for a $3dz^2$-based ground state

$$g_\perp - g_e = 6\zeta/\Delta_{xz/yz-z^2}$$

where ζ is the single electron spin−orbit coupling constant for cobalt (515 cm^{-1}) and $\Delta_{xz/yz-z^2}$ is the energy difference between the z^2-based ground state and a state described by the unpaired electron in the *xz*/*yz* orbitals.

For a $3d_{x^2-y^2}$-based ground state

$$g_\parallel - g_e = 8\zeta/\Delta_{xy-x^2-y^2}$$

$$g_\perp - g_e = 2\zeta/\Delta_{xz/yz-x^2-y^2}$$

where $\Delta_{xy-x^2-y^2}$ is the energy difference between the x^2-y^2-based ground state and a state described by the unpaired electron in an *xy*-based orbital; $\Delta_{xz/yz-x^2-y^2}$ is the energy difference between the x^2-y^2-based ground state and a state described by the unpaired electron in the *xz*/*yz* orbitals.

RESULTS

Synthesis and Structural Characterization. Analysis of X-ray quality crystals of **1** reveals a rigorously planar, 4-coordinate structure. When **1** is dissolved in CH_3CN, the slow diffusion of diethyl ether into the solution affords orange crystals, the X-ray diffraction analysis of which show a 6-

https://doi.org/10.1021/acs.inorgchem.2c01562
Inorg. Chem. 2022, 61, 12625−12634

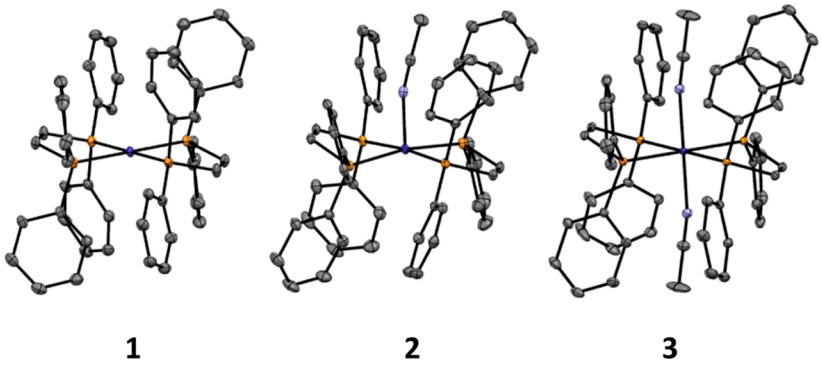

Figure 1. Structural representation of **1**, **2**, and **3** in the solid state with displacement ellipsoids shown at the 50% probability level. Hydrogen atoms and counter anions are omitted for clarity. Dark blue = Co, light blue = N, orange = P, and gray = C.

Table 1. Structural Parameters for Complexes 1, 2, and 3[a]

	Co−P bond distance (Å)				P−Co−P bite angle (deg)		dppv dihedral angle (deg)		*trans*-phosphine bond angle (deg)	
complex	P1	P2	P3	P4	P1/P2	P3/P4	P1/P2	P3/P4	P1/P3	P2/P4
1	2.282	2.281	2.281	2.282	83.45	83.45	1.31	1.31	180	180
2	2.277	2.291	2.314	2.272	82.65	84.21	4.96	3.96	174	171
3	2.332	2.318	2.318	2.332	82.04	82.04	2.65	2.65	180	180

[a]For **1**, P1 and P3 lie on symmetry elements which make the parameters equivalent.

coordinate complex with two CH_3CN ligands coordinated in the axial positions ($[Co(dppv)_2(NCCH_3)_2][BF_4]_2$, compound **3**). When the same recrystallization method is used (CH_3CN/ether) but in the presence of excess $NaBPh_4$, however, crystals of either a 5-coordinate complex with only a single CH_3CN ligand coordinated ($[Co(dppv)_2(NCCH_3)][BPh_4]_2$, compound **2**) or a similar 6-coordinate complex ($[Co(dppv)_2(NCCH_3)_2][BPh_4]_2$, compound **3b**) are isolated (Figure 1).

The crystal structure data from **1**, **2**, and **3** reveal subtle but distinct differences in bonding of the phosphine ligands among the series in the solid state (Table 1). For the two that are symmetric above and below the plane of the phosphine ligands, compounds **1** and **3**, the Co(II) sits directly in the center of the plane of the phosphorus atoms. This is apparent from the *trans*-phosphine bond angles being 180° for those complexes. In the 5-coordinate complex **2**, Co(II) is distorted out of the plane of the phosphorus ligands in the direction of the bound CH_3CN ligand. There is a slight elongation of the average Co−P bond as the coordination number increases. Additionally, for complex **2**, the two chelating phosphine ligands are more asymmetric with respect to each other than in complexes **1** and **3**. This is apparent in the differences in the P1/P2 versus P3/P4 bite angles and the differences in the dppv ligand dihedral angles on the same complex.

Strikingly, the 4-coordinate $[Co(dppv)_2]^{2+}$ is shown to be rigorously planar by X-ray crystallography. Several square-planar cobalt(II) complexes have been reported, but those contain higher-order hapticity ligands such as pincers (tridentate, neutral, or monoanionic),[19] porphyrins (tetradentate and dianionic),[20] or salens (tetradentate and dianionic).[21,22] There are rare examples of square-planar Co(II) complexes featuring bidentate ligands but only when those ligands are negatively charged (e.g. aminophenol).[23] To the best of our knowledge, this is the first crystallographically characterized square-planar Co(II) complex containing only neutral, bidentate ligands.

UV−Visible Spectroscopy. It was unclear from the solid-state structural data why the addition of $Na[BPh_4]$ results in the isolation of either 5- or 6- coordinate cobalt complexes from acetonitrile solutions. While there are no obvious structural interactions between BPh_4^- and the cobalt complex in the solid state, UV−visible absorbance spectroscopy was used to probe a possible equilibrium in solution.

Indeed, when $[TBA][BPh_4]$ (TBA = tetrabutylammonium; BPh_4 = tetraphenylborate) is titrated into a solution of $[Co(dppv)_2(NCCH_3)_2][BF_4]_2$ in CH_3CN, minor changes in the spectra are observed (Figure 2), and changes in the spectra

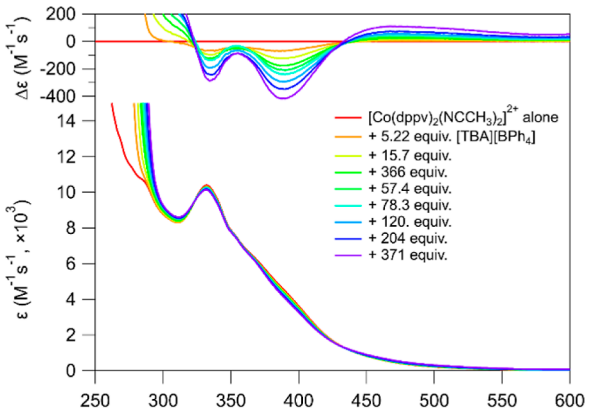

Figure 2. UV−visible absorbance spectra of the titration of $[TBA][BPh_4]$ into a solution of $[Co(dppv)_2(NCCH_3)_2][BF_4]_2$ in CH_3CN (TBA = tetrabutylammonium; BPh_4 = tetraphenylborate).

versus the concentration of added $[TBA][BPh_4]$ can be fit with a single equilibrium binding isotherm (see the Supporting Information). This indicates that there is some equilibrium in solution mediated by $[TBA][BPh_4]$, presumably the ligation and dissociation of a second CH_3CN ligand. This equilibrium explains why both 5- and 6-coordinate complexes were isolated when recrystallization occurred in the presence of BPh_4^-

https://doi.org/10.1021/acs.inorgchem.2c01562
Inorg. Chem. 2022, 61, 12625−12634

(Scheme 1). One plausible model is that the Co^{2+}/BPh_4^- ion pair is not as stable in acetonitrile as the Co^{2+}/BF_4^- ion pair.

Scheme 1. Ligation Chemistry of $[Co(dppv)_2]^{2+}$ under Various Conditions to form 4-, 5-, and 6-Coordinate Complexes

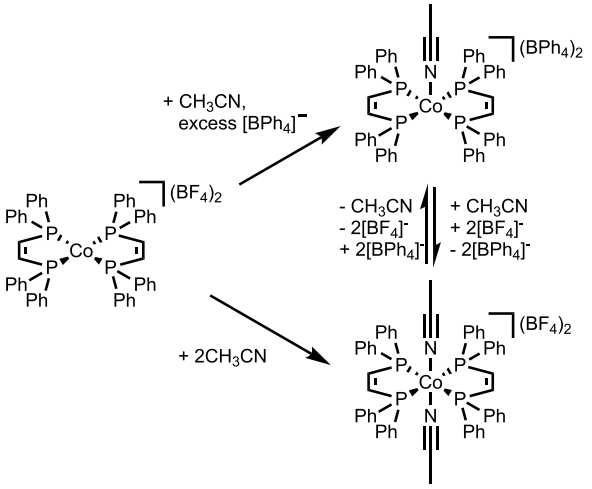

At high concentrations of BPh_4^-, the equilibrium is shifted to the 5-coordinate/BPh_4^- complex, presumably with binding of the phenyl group.[24] Consequently, one BF_4^- anion does mildly encroach on the pocket of the cobalt phosphine core in the 4-coordinate complex, indicating stronger ion pairing. This pairing is non-negligible in acetonitrile.[25]

EPR Characterization. All EPR spectra described below are consistent with mononuclear low-spin ($S = 1/2$) d^7 Co(II)-containing complexes. Depending on the ligand field, the ground electronic state single unpaired electron is found in either the $3dz^2$ or $3d_{x^2-y^2}$-based molecular orbital (vide infra).

The continuous-wave (CW) EPR spectrum of solid **1** (Figure 3A) is characterized by a rhombic g-tensor (g = [2.75, 2.47, 1.978]) and exhibits splitting attributed to a large magnitude ^{59}Co ($I = 7/2$) hyperfine interaction (HFI) (A^{59}Co = [490, 350, 350] MHz). These magnetic properties are consistent with the unquenched orbital angular momentum in the ground state owing to the high local symmetry of the cobalt spin-center in the square-planar ligand sphere. Further hyperfine splittings from the four ligating ^{31}P nuclei ($I = 1/2$) are not apparent, though it was convenient to model the spectral lineshape using four ^{31}P hyperfine tensors, A^{31}P = [125, 115, 55] MHz. These magnetic parameters are almost identical to those observed for $[Co(dppe)_2][ClO_4]_2$,[26] which was surmised to possess a $(d_{z^2})^1$ ground-state electron configuration.

No ^{59}Co HFI was resolved in the spectrum of the solid 4-coordinate complex **1** with added dppe (Figure 3B). The reported A^{59}Co values in Table 2 were chosen to model the non-Gaussian lineshape of the resonance; these values are likely upper bounds for the metal HFI. Spectra **3A** and **3B** are of crushed powders and are therefore likely distorted from ideality due to partial ordering and/or dipolar broadening.[27]

Dissolution of the 4-coordinate complex **1** (Figure 3C) into acetone results in a change in the EPR spectrum indicating coordination of a fifth ligand, likely a molecule of acetone, and analogous to earlier observations of solvent coordination in cobalt-corrinoids.[28] The axial g-tensor (with $g_\perp > g_\parallel \approx g_e$) and ^{59}Co hyperfine ($A_\parallel \gg A_\perp$) are indicative of a cobalt-based $3d_{z^2}$

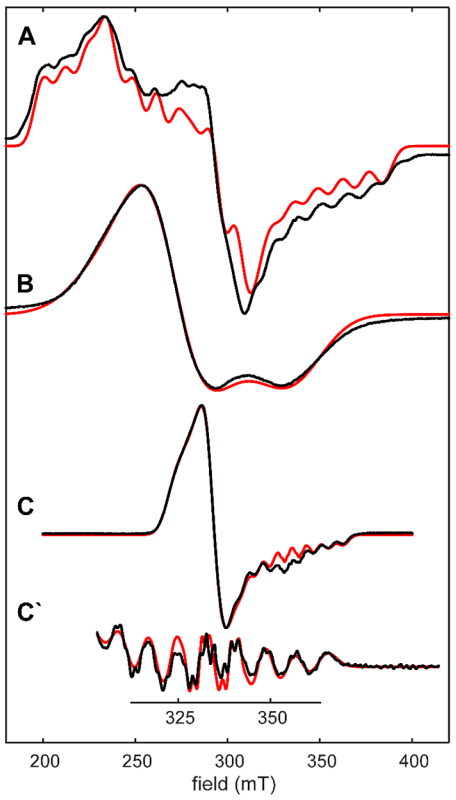

Figure 3. CW EPR spectra (black traces) of Co(II) complexes with various axial ligands. (A) Crushed powder of $[Co(dppv)_2][BF_4]_2$ (**1**), temperature = 77 K; (B) $[Co(dppv)_2][BF_4]_2$ (**1**) + dppe, temperature = 70 K; (C) frozen solution of $[Co(dppv)_2][BF_4]_2$ (**1**) in acetone, temperature = 10 K; (C′) computed numerical derivative showcasing the ^{31}P hyperfine coupling that is evident along $g_\parallel$. Spectrometer settings: (A) microwave frequency = 9.434 GHz, microwave power = 2 mW; (B) microwave frequency = 9.377 GHz, microwave power = 6.4 mW; (C) microwave frequency = 9.377 GHz, microwave power = 2 mW. Simulations (red traces) achieved with magnetic parameters given in Table 2 and these inhomogeneity parameters: (A) linewidth = 2 mT, g-strain = [0.08, 0.05, 0.06]; (B) linewidth = 31.4 mT, g-strain = [0.30, 0.05, 0.11]; (C) linewidth = 2 mT, g-strain = [0.036, 0.011, 0.00].

ground state. Using Pryce's perturbative formulas,[18] the prediction of g-shift from ligand-field splittings and a spin–orbit coupling constant for Co(II) of $\zeta = 515$ cm^{-1}, the xz/yz singly occupied excited state lies 9200 cm^{-1} above the ground state. We note that ζ is ∼90% of the free-ion value for Co(II), which is high for very covalent complexes. Values of 80−100% are routinely used for complexes of less covalency (such as square planar complexes), and often ζ is only accurate to within 10%.[29] Hyperfine coupling from the four equatorial ^{31}P ($I = 1/2$) ligand atoms is evident at the m_I −1/2 ↔ +1/2 resonances along $g_\parallel$ (c.a. 330 and 340 mT, Figure 3C). This was modeled as four identical isotropic couplings of 55 MHz. Note that only along $g_\parallel$ are these splittings resolved. Along the other g-axes, the tabulated ^{31}P HFI merely contributes to the line broadening and should not be considered accurate measures of the coupling along these dimensions.

The CW EPR spectrum of the solid, singly−CH_3CN−ligated 5-coordinate complex **2** (Figure 4A) is axial and reminiscent of many pseudo-C_{4v}-symmetric cobalamin and cobalt(II) porphyrin spectra with $g_\perp > g_\parallel \approx g_e$. The magnitude of the g-shift for $g_\perp$ corresponds to a $\Delta_{xz/yz-z^2} = 11{,}300$ cm^{-1}.

https://doi.org/10.1021/acs.inorgchem.2c01562
Inorg. Chem. 2022, 61, 12625−12634

Table 2. Magnetic Parameters for Cobalt-Phosphine Complexes[a]

complex	g	^{59}Co (MHz)	^{31}P (MHz)	refs
1 solid	[2.75, 2.47, 1.978]	[490, 350, 350]	[125, 115, 55]	this study
1 solid + dppe	[2.673, 2.508, 2.005]	[275, 47, 80]	n.d.	this study
1 in acetone	[2.400, 2.278, 1.999]	[99, 52, 220]	[55, 55, 55]	this study
2 solid	[2.290, 2.262, 2.009]	[12, 35, 212]	n.d.	this study
3 solid	[2.163, 2.159, 2.009]	[248, 278, 48]	n.d.	this study
3 solid + DPPE	[2.305, 2.230, 2.007]	[22, 31, 202]	n.d.	this study
3 in acetone	[2.298, 2.222, 2.005]	[31, 20, 206]	n.d.	this study
3 in CH_3CN	[2.154, 2.134, 1.999]	[275, 276, 29]	n.d.	this study
$[Co(dppe)_2][ClO_4]_2$	[2.797, 2.442, 1.968]	[482, 396, 402]	n.a.	26
$[Co(dppv)_2Br]^+$	[2.309, 2.239, 2.010]	[210, 42, 66]	[50, 50, 50]	30
$CoSal^{tBu\ NO2}$	[2.56, 2.30, 1.98]	[410, 196, 346]	n.a.	31

[a]n.d. Not detected. n.a. Not applicable.

As in the spectrum of the 4-coordinate complex dissolved in acetone, the $g_{\|}$ resonance is split into eight peaks owing to a strong ($A_{\|}$ = 212 MHz) HFI with the ^{59}Co nucleus along this dimension.

The 6-coordinate Co(II) complex **3** possesses two CH_3CN axial ligands leading to a significant alteration of the corresponding EPR spectrum (Figure 4B) compared to the 5-coordinate species. The g-tensor is still axial with $g_{\perp} > g_{\|} \approx g_e$, but the strong ^{59}Co hyperfine splitting is now observable along $g_{\perp}$, not along $g_{\|}$. This spectral change suggests a change in the ground-state orbital description for the unpaired electron from being housed in a cobalt-based $3d_{z^2}$ molecular orbital to one that is more $3d_{x^2-y^2}$ in character. Analysis of the g-values suggests that the xz/yz excited state lies ≈6500 cm^{-1} above the $x^2 - y^2$ ground state.

Addition of dppe (Figure 4C) reverts the spin system back to the $3dz^2$ ground state, as does dissolution of the complex in acetone (Figure 4D). However, dissolution of **3** in CH_3CN (Figure 4E) seems to maintain the $3d_{x^2-y^2}$ ground state, and the corresponding g-values and ^{59}Co HFI are very similar to those found for the solid 6-coordinate complex. This behavior suggests that the second CH_3CN axial ligand is maintained in CH_3CN solvent but is lost when the solvent is acetone. This loss of an axial ligand stabilizes the $3d_{z^2}$ orbital to an energy below that of $3d_{x^2-y^2}$, leading to its occupation by the unpaired electron.

Angular Overlap Model Calculations. The one electron orbital energy levels of **1**, **2**, and **3** were calculated by diagonalizing matrices of overlap integrals of the angular components of the d functions along with the parameterized energies of sigma (e_σ) and pi (e_π) interactions with the ligands.[32] For the equatorial dppv ligands, we used 4000 cm^{-1} (e_σ) and −2500 cm^{-1} (e_π) for each of the four P−Co interactions.[33] These are the reported[33] angular overlap model (AOM) parameters for triphenylphosphine, which are likely close to the (unmeasured) parameters for dppv. Ultimately, changing the absolute values of e_σ and e_π results only in a scaling relationship for our calculated orbital energies and does not affect the relative orderings. A P−Co−P "bite angle" of 83° was used for the equatorial ligand geometry since this is the average of the bite angles for **1** through **3** (σ = 0.9°).

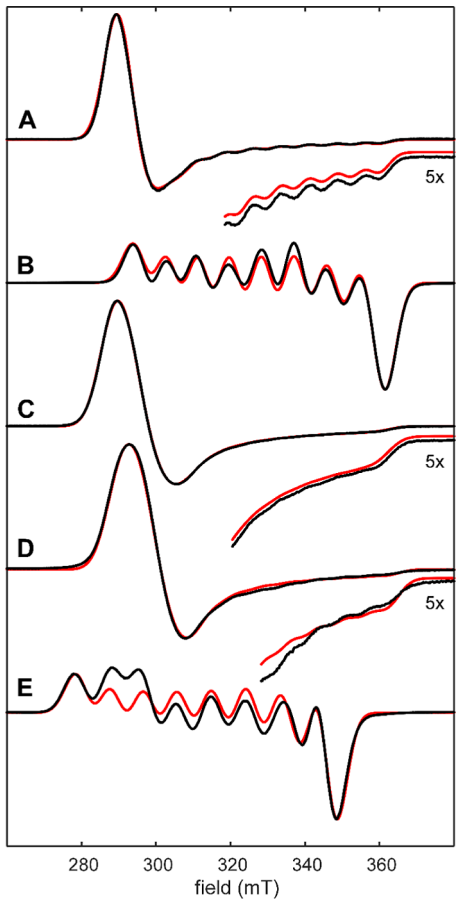

Figure 4. CW EPR spectra (black traces) of Co(II) complexes with various axial ligands. (A) Crushed powder of $[Co(dppv)_2(NCCH_3)][BPh_4]_2$, temperature = 4 K; (B) crushed powder of $[Co(dppv)_2(NCCH_3)_2][BPh_4]_2$, temperature = 77 K; (C) crushed powder of $[Co(dppv)_2(NCCH_3)_2][BPh_4]_2$ + dppe, temperature = 50 K. (D) Frozen solution of $[Co(dppv)_2(NCCH_3)_2][BPh_4]_2$ dissolved in acetone, temperature = 77 K; (E) frozen solution of $[Co(dppv)_2(NCCH_3)_2][BPh_4]_2$ dissolved in CH_3CN, temperature = 4 K. Spectrometer settings: (A) microwave frequency = 9.377 GHz, microwave power = 0.02 mW; (B) microwave frequency = 9.861 GHz, microwave power = 2 mW; (C) microwave frequency = 9.377 GHz, microwave power = 0.08 mW; (D) microwave frequency = 9.436 GHz, microwave power = 2 mW; (E) microwave frequency = 9.376 GHz, microwave power = 0.004 mW. Simulations (red traces) achieved with magnetic parameters given in Table 1 and these inhomogeneity parameters: (A) linewidth = 6.7 mT, g-strain = [0.026, 0.050, 0.007]; (B) linewidth = 6.4 mT, g-strain = [0.017, 0.023, 0.02]; (C) linewidth = 8.3 mT, g-strain = [0.013, 0.041, 0.027]; (D) linewidth = 8.0 mT, g-strain = [0.024, 0.046, 0.007]; (E) linewidth = 7.4 mT, g-strain = [0.00, 0.011, 0.0003]. Insets show spectra (black) and simulations (red) of $g_{\|}$ region for spectra B, D, and E, multiplied by a factor of 5 to better show the ^{59}Co hyperfine splittings.

One benefit of the AOM methodology is that the overlap integrals can be parameterized precisely.[34] Factoring energies in terms of the well-known Racah parameters A, B, and C requires some fundamental symmetry components to make the calculation feasible and meaningful;[35] unfortunately, the AOM model does not explicitly deal with the multielectron problem and configuration interaction. In the present case of a Co(II)

https://doi.org/10.1021/acs.inorgchem.2c01562
Inorg. Chem. 2022, 61, 12625−12634

center with an $S = 1/2$ ground state, configuration interaction does not significantly affect the energies of the lowest-energy doublet transitions. It should be noted, however, that more sophisticated perturbation treatments show non-negligible interactions between the doublet ground state and low-lying quartet states.[36] Additionally, a ligand field theory/AOM hybrid approach has been used to solve cases where interelectronic repulsion dominates [e.g., $S = 1$ Cr(II)].[37]

The full Mathematica[38] code to generate the enclosed plots is included in the Supporting Information.

DISCUSSION

Figure 5 presents the ligand field splitting (one-electron orbital energies) for the 6-coordinate complex **3**. The diagram was determined by considering (1) an electronic absorption at 1200 nm (8300 cm^{-1}) in the diffuse reflectance spectrum of solid **3**, (2) the existence of an xz/yz excited state 6500 cm^{-1} above the $x^2 - y^2$ ground state, and (3) a second, asymmetric ligand-field transition at 700 nm (14,300 cm^{-1}). Notably, the d_{z^2} orbital is close in energy to the $d_{x^2-y^2}$ orbital. This can be predicted by EPR spectroscopy, which shows that the ground state changes going from 5-coordinate to 6-coordinate. We believe that this is the primary reason for axial ambivalence: a small energy gap allows for the crossing of the two frontier orbitals with increasing axial contribution. Occupation of the $d_{x^2-y^2}$ orbital would therefore encourage axial binding, while occupation of the d_{z^2} orbital would favor axial ligand loss (d_{z^2} is σ^* with respect to ligands along the primary rotation axis, z). Furthermore, we know that the ground state is $(d_{z^2})^1$ for **1** and **2** (owing to an axially symmetric EPR spectrum, with the largest element of the ^{59}Co HFI appearing along $g_{||}$), which places the crossover point somewhere between the geometries of complexes **2** and **3**. From this perspective, the significant geometric distortion of complex **2** is likely explained by a second-order Jahn–Teller effect in which vibrations are coupled to a low-lying excited state.[39] Using the AOM model, we can generate the one-electron orbital energies as we progress from 4-coordinate to 5-coordinate to 6-coordinate (Figure 6).

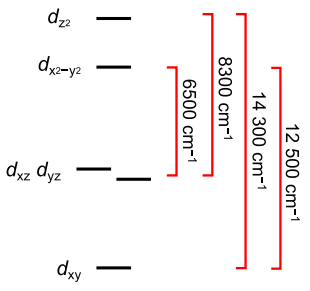

Figure 5. Ligand-field splitting diagram illustrating the electronic structure of the pseudo-octahedral **3** (6-coordinate) complex. The diagram is consistent with both EPR and electronic absorption spectroscopies, including the presence of a weak band at 1200 nm (8300 cm^{-1}), which is seen in the NIR diffuse reflectance spectrum of solid **3**. Other magnitudes are derived from the g-values in the EPR analysis (above).

Notably, these calculations confirm the prediction of a crossover point in the energy diagram. The energies of the $d_{x^2-y^2}$ and d_{z^2} orbitals are independent of the axial e_π component because of the orthogonality of those orbitals with the π symmetry orbitals of the axial ligand. The crossover is calculated at e_σ(axial) ≈ 8000 cm^{-1}. In terms of only radial

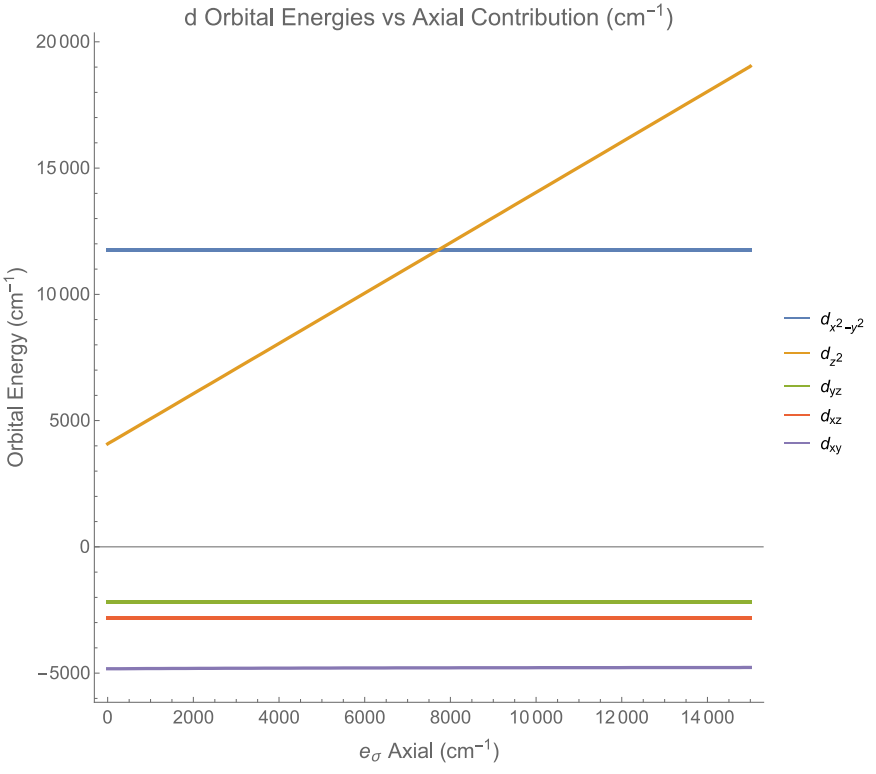

Figure 6. One-electron orbital energies of the d orbitals as a function of the axial electronic interaction e_σ. Note that the e_π component of the axial ligands does not affect the energies of the two highest energy levels because of orthogonality. The lower levels are slightly dependent on the axial e_π, but this interaction is removed for clarity. Here, e_σ is treated as the sum of the two axial acetonitrile interactions.

https://doi.org/10.1021/acs.inorgchem.2c01562
Inorg. Chem. 2022, 61, 12625−12634

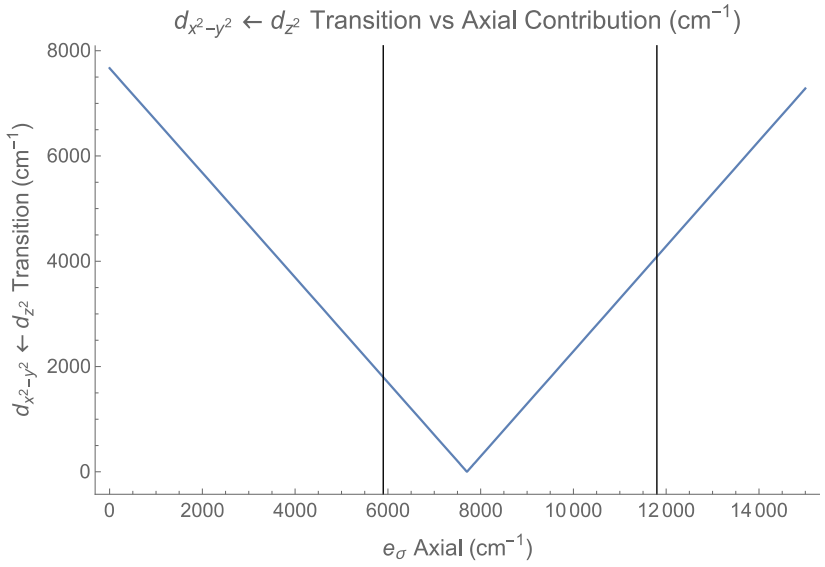

Figure 7. Locations of the 5- and 6-coordinate complexes (vertical lines) while visualizing the $d_{z^2}/d_{x^2-y^2}$ energy gap in terms of e_σ axial. The 5-coordinate complex **2** gives an exact value for e_σ(MeCN), while the 6-coordinate complex **3** can be approximated as < $2e_\sigma$(MeCN) due to elongation of the Co−N bonds in **3**.

functions, e_σ is treated as the sum of two axial acetonitrile interactions. The energy gap between d_{z^2} and $d_{x^2-y^2}$ for **3** is ∼1800 cm^{-1}, so the gap between d_{z^2} and $d_{x^2-y^2}$ for **2** must be <1800 cm^{-1}. By plotting the transition or "cross-over" energy versus e_σ(axial), we can calculate that $e_\sigma(CH_3CN)$ is ∼5900 cm^{-1} (Figure 7). This is a reasonable value of $e_\sigma(CH_3CN)$ but indicates that acetonitrile is a better σ-donor than typically thought.[40] It is important to emphasize that e_σ is bond length-dependent (radial integrals are not considered in AOM). Therefore, while $e_\sigma(CH_3CN, @\ 2\ Å)$ is calculated to be 5900 cm^{-1} (5-coordinate), $e_\sigma(CH_3CN, @\ 2.1\ Å)$ will be much smaller (6-coordinate). The splitting determined by EPR (∼2000 cm^{-1}) validates the notion that binding two axial acetonitrile molecules does not double the σ interaction. A general rule-of-thumb is that the lengthening of a bond by ∼0.1 Å indicates a change in the antibonding level by ∼10 Dq/Δ_o; this is the equivalent of adding one antibonding electron. Thus, we conclude that $e_\sigma(CH_3CN, @\ 2\ Å) \approx 2e_\sigma(CH_3CN, @\ 2.1\ Å)$.

For the sake of completeness, we note that complexes cannot exist within $\pm\ \lambda$ of the crossover, where λ is the reorganization energy. This so-called "forbidden region," which arises from the fact that bond lengths are quantized in spin- and orbital−state transitions, is also applicable in Tanabe−Sugano diagrams for multielectron states.[41] This exclusion region primarily affects our predicted location of **2** relative to the crossover point since λ may be larger than 1800 cm^{-1}, as assumed above. If the value of λ is greater than 1800 cm^{-1}, e_σ(MeCN) would necessarily be smaller as **2** moves away from the crossover point. Therefore, 5900 cm^{-1} is an upper-bound for e_σ(MeCN).

The above calculations depend only on the values of e_σ and e_π for the phosphine ligands. (At 90° there is no e_π contribution, using a similar argument as for the axial π interaction.) What happens as the values of e_σ and e_π for the four equatorial ligands change? We can perform these calculations analytically. The most informative calculations are those that minimize the $d_{z^2}/d_{x^2-y^2}$ energy gap because those would describe complexes at (or near) the crossover point between 5- and 6-coordination numbers. Thus, by knowing the appropriate equatorial ligand parameters of the square-planar core—phosphines or otherwise—we can predict whether potential substrates would be axially labile.

To visualize the results of these calculations, we generated contour plots that relate any combination of equatorial e_σ and e_π values of the square-planar core to the e_σ (axial) values of potential axial ligands that would be predicted to yield "axial ambivalent" complexes. Thus, by following a contour of a specific axial ligand sigma-donor strength, the corresponding values of the equatorial ligands that would be required for labile axial binding become apparent (Figure 8). Plots are shown for three different equatorial bidentate ligand "bite angles": 75, 83, and 90°. Interestingly, smaller bite angles cause significant distortions of the contours due to mixing of orbitals of π symmetry. Thus, in addition to modifying the σ-only strength of the equatorial ligands, one might also consider building scaffolds with varying "bites." The large range of σ-donation and π-acceptor abilities of various phosphines has previously been explored.[42]

These contour plots provide a methodology for developing cobalt complexes which will reversibly bind a variety of substrates. We might be very interested in engineering cobalt cores which will preferentially bind some substrates over others. For example, how can we use these plots to explore complexes suitable for dinitrogen reduction in aqueous solutions? The axial sigma interaction [e_σ (axial)] of dinitrogen bound end-on has been estimated to be 6900 cm^{-1}.[43] With an 83° bite angle, e_σ(equatorial) for the square-planar core should be ∼4750 cm^{-1}, a slightly weaker sigma-donor than dppv. With a tighter "bite angle," e_σ(equatorial) could be as large as 5000 cm^{-1} if there were a small-to-moderate e_π(equatorial) contribution.

A major problem in dinitrogen reduction catalysis, however, is the simultaneous reduction of protons in aqueous solution. In the case of preferentially binding dinitrogen (rather than protons/hydrides), one quickly realizes that due to the lack of e_π variation in the plots, one cannot preferentially bind a weaker σ-donor. This is made apparent by the monotonic

https://doi.org/10.1021/acs.inorgchem.2c01562
Inorg. Chem. 2022, 61, 12625−12634

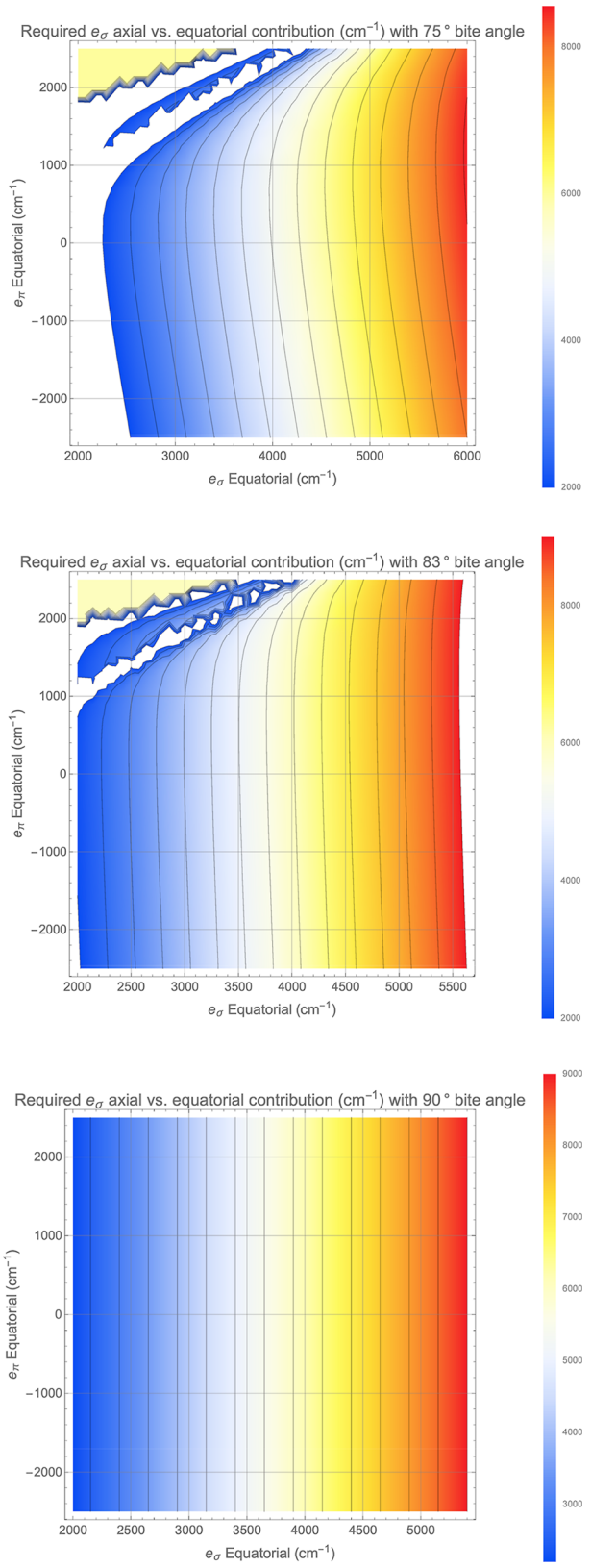

Figure 8. Contour plots that minimize the $d_{z^2}/d_{x^2-y^2}$ energy gap as a function of e_σ and e_π of the equatorial phosphines. Color indicates the magnitude of the axial e_σ (total) at the minimum. White areas indicate regions where other crossings have occurred and the $d_{z^2}/d_{x^2-y^2}$ transition is no longer relevant. Different "bite angles" of the phosphine ligands are calculated; (top) 75°, (middle) 83° (the average "bite angle" of dppv), and (bottom) 90°.

nature of the plots in Figure 8. One can show that this is true for any tetragonal geometry. As such, trigonal or otherwise significantly distorted complexes are of particular interest due to the admixture of states. Extending the model to include low-symmetry complexes is an ongoing work.

CONCLUSIONS

We report here the structural and spectroscopic characterization of a series of cobalt complexes that are 4-, 5-, and 6-coordinate with the same $Co(dppv)_2^{2+}$ core. The 4-coordinate complex was isolated from acetone, while the 5- and 6-coordinate complexes were isolated from acetonitrile in the presence of and in the absence of BPh_4^-, respectively. Titration of BPh_4^- salt into a solution of the isolated 6-coordinated complex in acetonitrile shows subtle changes to the UV−vis spectrum, indicating an equilibrium between 6- and 5-coordinate species in solution. The crystal structures of each complex are reported, which includes a very rare example of a rigorously planar 4-coordinate cobalt(II) complex with neutral ligands. EPR spectroscopic results reveal that there is a change in the ground-state electronic configuration between the 5- and 6-coordinate structures; AOM calculations suggest readily tunable ligand parameters for accessing this "axial ambivalent" region for any potential axial-ligand substrate. A series of diagrams are provided that can assist in the intelligent design of equatorial phosphines (or any other scaffold) that will make catalytically relevant small molecules labile.

ASSOCIATED CONTENT

Supporting Information

The Supporting Information is available free of charge at https://pubs.acs.org/doi/10.1021/acs.inorgchem.2c01562.

Change in molar extinction coefficient at 390 nm as a function of added $[TBA][BPh_4]$ to a solution of $[Co(dppv)_2(NCCH_3)_2][BF_4]$ in CH_3CN and binding isotherm fit showing that an equilibrium is present; UV−visible reflectance spectra of **1**, **2**, and **3**; and cobalt II AOM calculations (PDF)

Accession Codes

CCDC 2166489−2166490 contain the supplementary crystallographic data for this paper. These data can be obtained free of charge via www.ccdc.cam.ac.uk/data_request/cif, or by emailing data_request@ccdc.cam.ac.uk, or by contacting The Cambridge Crystallographic Data Centre, 12 Union Road, Cambridge CB2 1EZ, UK; fax: +44 1223 336033.

AUTHOR INFORMATION

Corresponding Author

Bryan M. Hunter − *Rowland Institute at Harvard University, Cambridge, Massachusetts 02142, United States;* orcid.org/0000-0001-8559-9304; Email: bhunter@rowland.harvard.edu

Authors

Jack Thomas-Colwell − *Department of Chemistry, Occidental College, Los Angeles, California 90041, United States*

Arvin Sookezian − *Department of Chemistry, Occidental College, Los Angeles, California 90041, United States*

Daniel A. Kurtz − *Rowland Institute at Harvard University, Cambridge, Massachusetts 02142, United States;* orcid.org/0000-0002-0082-1699

Jeremy Kallick − *Department of Chemistry, Occidental College, Los Angeles, California 90041, United States*
Lawrence M. Henling − *Division of Chemistry and Chemical Engineering, California Institute of Technology, Pasadena, California 91125, United States*
Troy A. Stich − *Department of Chemistry, Wake Forest University, Winston−Salem, North Carolina 27109, United States;* orcid.org/0000-0003-0710-1456
Michael G. Hill − *Department of Chemistry, Occidental College, Los Angeles, California 90041, United States*

Complete contact information is available at: https://pubs.acs.org/10.1021/acs.inorgchem.2c01562

Notes

The authors declare no competing financial interest.

■ ACKNOWLEDGMENTS

D.A.K. thanks the Rowland Foundation, Inc. For a Rowland Postdoctoral Fellowship. B.M.H. is a Fellow of the Rowland Institute at Harvard. T.A.S. thanks the Wake Forest University for the financial support. The Bruker D8 Kappa X-ray diffractometer was purchased via an NSF CRIF:MU award to the California Institute of Technology (CHE-0639094).

■ REFERENCES

(1) Haynes, W. M.; Lide, D. R.; Bruno, T. J. *CRC Handbook of Chemistry and Physics*; CRC press, 2016.
(2) Chirik, P. J. Iron- and Cobalt-Catalyzed Alkene Hydrogenation: Catalysis with Both Redox-Active and Strong Field Ligands. *Acc. Chem. Res.* **2015**, *48*, 1687−1695.
(3) Kohler, L.; Niklas, J.; Johnson, R. C.; Zeller, M.; Poluektov, O. G.; Mulfort, K. L. Molecular Cobalt Catalysts for H_2 Generation with Redox Activity and Proton Relays in the Second Coordination Sphere. *Inorg. Chem.* **2019**, *58*, 1697−1709.
(4) Kurtz, D. A.; Dhar, D.; Elgrishi, N.; Kandemir, B.; McWilliams, S. F.; Howland, W. C.; Chen, C.-H.; Dempsey, J. L. Redox-Induced Structural Reorganization Dictates Kinetics of Cobalt(III) Hydride Formation via Proton-Coupled Electron Transfer. *J. Am. Chem. Soc.* **2021**, *143*, 3393−3406.
(5) Dempsey, J. L.; Brunschwig, B. S.; Winkler, J. R.; Gray, H. B. Hydrogen Evolution Catalyzed by Cobaloximes. *Acc. Chem. Res.* **2009**, *42*, 1995−2004.
(6) Cole-Hamilton, D. J. Homogeneous Catalysis–New Approaches to Catalyst Separation, Recovery, and Recycling. *Science* **2003**, *299*, 1702−1706.
(7) Vaska, L. Oxygen-Carrying Properties of a Simple Synthetic System. *Science* **1963**, *140*, 809−810.
(8) Miskowski, V. M.; Robbins, J. L.; Hammond, G. S.; Gray, H. B. Preparation and spectroscopic properties of cobalt (III) complexes containing phosphine ligands. The electronic structural description of side-bonded dioxygen. *J. Am. Chem. Soc.* **1976**, *98*, 2477−2483.
(9) Groom, C. R.; Bruno, I. J.; Lightfoot, M. P.; Ward, S. C. The Cambridge Structural Database. *Acta Crystallogr. B* **2016**, *72*, 171−179.
(10) Williams, A. F. Structures of bis(1,2-diphenylphosphinoethane)nickel(II) dinitrate and bis(cis-1,2-diphenylphosphinoethene)nickel(II) perchlorate. *Acta Crystallogr. C* **1989**, *45*, 1002−1005.
(11) Kurtz, D. A.; Zhang, J.; Sookezian, A.; Kallick, J.; Hill, M. G.; Hunter, B. M. A Cobalt Phosphine Complex in Five Oxidation States. *Inorg. Chem.* **2021**, *60*, 17445−17449.
(12) Langford, C.; Billig, E.; Shupack, S.; Gray, H. B. Interconvertible Four-, Five-, and Six-Coordinate Cobalt Complexes. *J. Am. Chem. Soc.* **1964**, *86*, 2958−2959.
(13) Bruker. *APEX3*; Bruker AXS Inc.: Madison, Wisconsin, USA, 2012.
(14) Bruker. *SADABS*; Bruker AXS Inc.: Madison, Wisconsin, USA, 2001.
(15) Sheldrick, G. M. SHELXT−Integrated space-group and crystal-structure determination. *Acta Crystallogr., Sect. A: Found. Adv.* **2015**, *71*, 3−8.
(16) Sheldrick, G. M. Crystal structure refinement with SHELXL. *Acta Crystallogr., Sect. C: Struct. Chem.* **2015**, *71*, 3−8.
(17) Stoll, S.; Schweiger, A. EasySpin, a comprehensive software package for spectral simulation and analysis in EPR. *J. Magn. Reson.* **2006**, *178*, 42−55.
(18) Pryce, M. H. L. A Modified Perturbation Procedure for a Problem in Paramagnetism. *Proc. Phys. Soc.* **1950**, *63*, 25−29.
(19) Rozenel, S. S.; Padilla, R.; Arnold, J. Chemistry of Reduced Monomeric and Dimeric Cobalt Complexes Supported by a PNP Pincer Ligand. *Inorg. Chem.* **2013**, *52*, 11544−11550.
(20) Yuzo, N.; Sigeo, K. Ground States of the Square Planar Low-Spin Cobalt(II) Complexes. *Bull. Chem. Soc. Jpn.* **1978**, *51*, 143−149.
(21) Cibian, M.; Derossi, S.; Hanan, G. S. Synthesis and crystal structure of a rare square-planar Co(ii) complex of a hydroxyamidinate ligand. *Dalton Trans.* **2011**, *40*, 1038−1040.
(22) Welby, J.; Rusere, L. N.; Tanski, J. M.; Tyler, L. A. Syntheses and crystal structures of mono-, di- and trinuclear cobalt complexes of a salen type ligand. *Inorg. Chim. Acta* **2009**, *362*, 1405−1411.
(23) Loginova, N. V.; Koval'chuk, T. V.; Osipovich, N. P.; Polozov, G. I.; Sorokin, V. L.; Chernyavskaya, A. A.; Shadyro, O. I. Redox-active antifungal cobalt(II) and copper(II) complexes with sterically hindered o-aminophenol derivatives. *Polyhedron* **2008**, *27*, 985−991.
(24) Ma, J. C.; Dougherty, D. A. The Cation−π Interaction. *Chem. Rev.* **1997**, *97*, 1303−1324.
(25) Freedman, D. A.; Matachek, J. R.; Mann, K. R. Ion pairing effects in the photochemistry of the cyclopentadienyl(η^6-benzene)-osmium(II) cation. Synthesis and reactions of a synthetically useful intermediate: the cyclopentadienyltris(acetonitrile)osmium(II) cation. *Inorg. Chem.* **1993**, *32*, 1078−1080.
(26) Nishida, Y.; Kida, S. ESR and spectral studies of bis-(ethylenebis(diphenylphosphine))cobalt(II) perchlorate. *J. Inorg. Nucl. Chem.* **1978**, *40*, 1331−1333.
(27) Stoll, S. CW-EPR Spectral Simulations: Solid State. In *Methods in Enzymology*; Qin, P. Z., Warncke, K., Eds.; Academic Press, 2015; Chapter 6, Vol. *563*, pp 121−142.
(28) Van Doorslaer, S.; Jeschke, G.; Epel, B.; Goldfarb, D.; Eichel, R.-A.; Kräutler, B.; Schweiger, A. Axial Solvent Coordination in "Base-Off" Cob(II)alamin and Related Co(II)-Corrinates Revealed by 2D-EPR. *J. Am. Chem. Soc.* **2003**, *125*, 5915−5927.
(29) Cole, G. M., Jr; Garrett, B. B. Atomic and molecular spin-orbit coupling constants for 3d transition metal ions. *Inorg. Chem.* **1970**, *9*, 1898−1902.
(30) Sethulakshmi, C.; Manoharan, P. EPR and electronic structural investigations of a few low-spin bis (tertiary phosphine) complexes of cobalt (II). *Inorg. Chem.* **1981**, *20*, 2533−2539.
(31) Chiang, L.; Allan, L. E. N.; Alcantara, J.; Wang, M. C. P.; Storr, T.; Shaver, M. P. Tuning ligand electronics and peripheral substitution on cobalt salen complexes: structure and polymerisation activity. *Dalton Trans.* **2014**, *43*, 4295−4304.
(32) Schäffer, C. E.; Jørgensen, C. K. The angular overlap model, an attempt to revive the ligand field approaches. *Mol. Phys.* **1965**, *9*, 401−412.
(33) Davies, J. E.; Gerloch, M.; Phillips, D. J. Phosphine π-acceptor properties in dihalogenobis (triphenylphosphine)-nickel (II) and-cobalt (II). *J. Chem. Soc., Dalton Trans.* **1979**, *11*, 1836−1842.
(34) Larsen, E.; La Mar, G. N. The angular overlap model. How to use it and why. *J. Chem. Educ.* **1974**, *51*, 633.
(35) Underhill, A. E.; Billing, D. E. Calculations of the Racah Parameter B for Nickel (II) and Cobalt (II) Compounds. *Nature* **1966**, *210*, 834−835.
(36) McGarvey, B. R. Theory of the Spin Hamiltonian Parameters for Low Spin Cobalt(II) Complexes. *Can. J. Chem.* **1975**, *53*, 2498−2511.

(37) Zolnhofer, E. M.; Opalade, A. A.; Jackson, T. A.; Heinemann, F. W.; Meyer, K.; Krzystek, J.; Ozarowski, A.; Telser, J. Electronic Structure and Magnetic Properties of a Low-Spin Cr^{II} Complex: trans-$[CrCl_2(dmpe)_2]$ (dmpe = 1,2-Bis(dimethylphosphino)ethane). *Inorg. Chem.* **2021**, *60*, 17865−17877.
(38) Wolfram Research. *I. Mathematica*; Wolfram Research, Inc.: Champaign, Illinois, 2021.
(39) Pearson, R. G. The second-order Jahn-Teller effect. *J. Mol. Struct.* **1983**, *103*, 25−34.
(40) Soukup, R. W.; Schmid, R. Metal complexes as color indicators for solvent parameters. *J. Chem. Educ.* **1985**, *62*, 459.
(41) Winkler, J. R.; Gray, H. B. Electronic Structures of Oxo-Metal Ions. In *Molecular Electronic Structures of Transition Metal Complexes I*; Mingos, D. M. P., Day, P., Dahl, J. P., Eds.; Springer Berlin Heidelberg: Berlin, Heidelberg, 2012; pp 17−28.
(42) Rahman, M. M.; Liu, H. Y.; Eriks, K.; Prock, A.; Giering, W. P. Quantitative analysis of ligand effects. Part 3. Separation of phosphorus (III) ligands into pure σ-donors and σ-donor/π-acceptors. Comparison of basicity and σ-donicity. *Organometallics* **1989**, *8*, 1−7.
(43) Lehnert, N.; Tuczek, F. The Reduction Pathway of End-on Coordinated Dinitrogen. II. Electronic Structure and Reactivity of Mo/W−N_2, −NNH, and −NNH_2 Complexes. *Inorg. Chem.* **1999**, *38*, 1671−1682.

https://doi.org/10.1021/acs.inorgchem.2c01562
Inorg. Chem. 2022, 61, 12625−12634